Neurobiology of Stress 34 (2025) 100677

Contents lists available at ScienceDirect

Neurobiology of Stress

journal homepage: www.elsevier.com/locate/ynstr

Emotional salience network involved in constructing two-dimensional fear space in humans☆

Jing Lyu [a,1], Jiayue Li [a,1], Rui Ding [a,1], Hui Zhao [a,**], Chao Liu [a,***], Shaozheng Qin [a,b,c,*]

[a] State Key Laboratory of Cognitive Neuroscience and Learning, Beijing Normal University, Beijing 100875, China
[b] IDG / Mc Govern Institute for Brain Research, Beijing Normal University, China
[c] Beijing Key Lab of Brain Imaging and Connectomics, Beijing Normal University, China

ARTICLE INFO

Handling Editor: Rita Valentino

Keywords:
Emotion
Salience
Fear space

ABSTRACT

Fear learning is pivotal for organismal survival, ensuring the ability to avoid potential threats through learning based on experiencing minimal fear information. In reality, fear learning requires to form a structured representation of fear experiences from multiple dimensions in order to support flexible use in ever-changing environment. Yet, the underlying neural mechanisms of constructing dimensional fear space remain elusive. Here we set up an innovative approach with two-dimensional fear learning, by utilizing the probability (uncertainty) and subjective pain intensity of threatening mild electric shock with five levels of each dimension. Behaviorally, individuals constructed a two-dimensional fear space after learning phase, as evidenced by significant changes in participant's fearful ratings for each cue associated with a five-by-five grid after (relative to before) learning phase. Analysis of neuroimaging data revealed that the medial temporal lobe, in conjunction with the amygdala, the insula, the anterior cingulate cortex (ACC), the hippocampus, and the dorsolateral prefrontal cortex (dlPFC), collectively contribute to the construction of a two-dimensional fear space consisting of uncertainty and intensity. Activation in the parahippocampal gyrus, insula, and dlPFC was associated with mental navigation within two-dimensional fear space, whereas the engagement of insula, ACC, amygdala, the hippocampus, the dlPFC was associated with a unified fearful scoring cross uncertainty and intensity dimensions after fear learning. Our findings suggest a neurocognitive model through which emotional salience network underlies the construction of a structured representation of fear experiences from multiple dimensions.

1. Introduction

Fear learning serves as a pivotal survival mechanism for organisms. Through a limited exposure to fear-inducing stimuli, individuals acquire the ability to evade potential threats, significantly enhancing their chances of survival (Dunsmoor and Paz, 2015). While previous quantitative studies have predominantly concentrated on fear conditioning or learning with cues (Bilodeau et al., 2023; Dou et al., 2023; Zoladz et al., 2023), real-life instances often involve the simultaneous association of multiple elements with fear. Thus, there is a need to delve into learning of multidimensional features. In both the natural world and human society, threats abound, and the capacity to detect and navigate these threats have become a critical factor for individual survival amidst ongoing crises (Bloom, 2004).

The Pavlovian fear conditioning has been the fundamental mechanism underlying fear and threat learning (Beckers et al., 2023; Boddez et al., 2020; Domjan, 2005). Simply put, it involves the pairing of a neutral conditioned stimulus (CS) with a negative unconditional stimulus (US) to facilitate multiple learning associations, thereby establishing a conditioned reflex (CR) eliciting a negative response (Feigenberg, 2014). Through such procedure, individuals can learn the association between simple sensory stimuli and aversive unconditioned stimuli like

☆ Data are available upon reasonable request.

* Corresponding author. State Key Laboratory of Cognitive Neuroscience and Learning, Beijing Normal University, Beijing, 100875, China.
** Corresponding author.
*** Corresponding author.
E-mail addresses: huizhao@bnu.edu.cn (H. Zhao), liuchao@bnu.edu.cn (C. Liu), szqin@bnu.edu.cn (S. Qin).
[1] Jing Lyu, Jiayue Li, and Rui Ding contributed equally to this work.

https://doi.org/10.1016/j.ynstr.2024.100677
Received 1 January 2024; Received in revised form 20 June 2024; Accepted 2 October 2024
Available online 11 October 2024

electric shocks. And numerous studies have successfully unveiled the learning mechanism underlying the fear acquisition for neutral stimuli, especially for single-dimensional ones (e.g. cue of single shape/object) (Glenn et al., 2012; Pattwell et al., 2012; Rau et al., 2005). Furthermore, the conditioned feature of varying levels (e.g. different size of the shape) can also be linked to varying intensities of unconditioned stimuli (Lissek et al., 2008, 2014), through which both humans and animals can construct linear relationship between conditioned feature levels and actual fear intensities (Dacey, 2019; Haselgrove, 2016; Mitchell et al., 2009). Reasoning about the relationship between conditioned and unconditioned stimuli can produce fear generalization (Beckers et al., 2023; Domjan, 2005; McNally and Westbrook, 2006), and generalize the limited fear learning to a wider range (Dunsmoor and Paz, 2015; Dymond et al., 2015). Despite the in-depth exploration of fear learning in the context of single-dimensional and multi-level conditioned stimuli, the traditional research largely ignores the situational complexity with multi-dimenstional features in shaping fear responses, and cannot satisfy the demand for adaptations to the complex environments in real-life instances. Thus, it still remains inadequate regarding how mechanisms of fear learning are formed and generalized in the context of multi-dimensional features.

In terms of the neural substrates underlying fear learning and generalization, previous studies have revealed essential contributions from structures covering cortical and subcotrical regions, including amygdala, hippocampus, EC, dlPFC, anterior insula (AI) and anterior/middle cingulate cortex (A/MCC) etc (Bissière et al., 2008; LeDoux and Pine, 2016; Ridderbusch et al., 2021; Rogan et al., 1997; Takehara, 2014; Veit et al., 2012; White et al., 2023; Yosephi et al., 2019). The amygdala and hippocampus, indicated by the long-term potentiation (LTP), play pivotal role in the acquisition, storage, and expression of conditioned fear memories (Kim and Jung, 2006; Rogan et al., 1997). The EC, being structurally projected into the hippocampus, has also been confirmed the involvement within the acquisition, consolidation, and retrieval of new memories (Basu et al., 2016; Maass et al., 2014; Takehara, 2014). Cortical regions, like dlPFC, AI and A/MCC, contribute to fear learning as well as fear generalization primarily through detection and regulation processing, during which attention is enhanced towards fear information, and fear response is adjusted in response to contexts (Bishop et al., 2004; Krolak et al., 2003; Peers et al., 2013; Vogt, 2019; Vuilleumier et al., 2003). Taken together, fear information processed in amygdala is sent to the salience network which helps assign significance/value to the paired unconditioned stimuli through integrative coordination of multiple regions and in turn promoting the encoding of fear memories (Cunningham and Brosch, 2012; Yin et al., 2018). Meanwhile, the salience network is also implicated in determining the similarity between novel stimuli and previously learned cues, and assists fear generalization to the similar but unseen contexts (Berg et al., 2021; dos Santos Corrêa et al., 2022). It is apparent that fear learning and generalization are intricately linked to the collaboration among core brain regions of emotion, memory, and the salience network. Here, we refer to this large-scale interactive network as the emotional salience network. These findings offer a comprehensive understanding for the neurocognitive mechanism underlying fear acquisition and generalization. However, these are mainly derived from the studies that have focused on single dimensional feature of conditioned stimulus, and it is not clear whether the multidimensional fear space acquired from the associative learning also follows the above mechanisms.

To address these open questions, we set up a functional magnetic resonance imaging (fMRI) study with a two-dimensional fear learning paradigm, by utilizing the probability (uncertainty) and subjective pain intensity of threatening mild electric shock with five levels of each dimension in an innovative design. Through such design, we endeavored to construct two-dimensional fear space within individuals, meanwhile to identify the neural network responsible for the navigation within the fear space. This was motivated by the basic associative learning theory (e.g. Pavlovian fear conditioning), which posits that pairing a fearful stimulus with a neutral stimulus will lead to the successful learning of fear towards the stimulus and also can be generalized to similar stimuli. Such procedure was done for each dimension of fear features, which in our study refers to the length of virus head spike and size of virus circle respectively linked to the intensity and probability of electrical shock (Fig. 1). The dimensions could be combined into a unified symbol (virus), and hypothesized that individuals can develop an internal two-dimensional fear representations which can be generalized to adjacent but unseen representational locations to form a complete fear space. Given the valuation of fear stimuli and the combination of two dimensions, we further expected the navigation within fear space would engage emotional salience network (e.g. amygdala, insula, cingulate cortex and prefrontal cortex) and memory laden regions (e.g. hippocampus and EC).

2. Methods and materials

2.1. Participants

A total of 72 participants took part in this study. Fifty of them engaged in various categories of pre-experiments, offering valuable references for the subsequent formal experiments, while 22 individuals participated directly in the final formal experiments. Within the formal experiment group, there were 10 male and 12 female participants, with an average age of 22.4 years. We conducted analyses on 22 behavioral data and 25 fMRI data, which included data from three pre-experiment subjects. Unfortunately, due to technical problems, data from two subjects were not available, so the final fMRI data were only 23. The participants were exclusively recruited from Beijing Normal University in Beijing, China. All participants were native Mandarin speakers with either normal vision or corrected-to-normal vision and exhibited no intellectual, behavioral, or sensory deficits. Prior to the commencement of the experiment, explicit permission was obtained from the school administration. And all participants signed an informed consent form.

2.2. Experimental stimulus

2.2.1. Fear stimulus

In this study, a Stimulus Isolation Adaptor (model STMISOC) manufactured by BIOPAC was employed to administer electrical stimulation. The shock stimulation generated a direct current square wave ranging from 0 to 100V, lasting 2 ms. Under dry conditions, the human body's resistance can reach up to 100 kΩ. High voltage can rapidly disrupt the original resistance of human skin, reducing it to a minimum of 500Ω (under 100V conditions, 95% of people can be reduced to less than 3200Ω, while 5% can be reduced to less than 1200Ω) (Reilly, 1998). Using a calculation based on 500Ω, the highest energy output of a single shock (J) = ((100V × 100V)/500Ω) × 0.002s = 40 mJ, significantly lower than the international standard for nerve and muscle stimulation (IEC 60601-2-10:2015), which mandates a single muscle shock pulse below 300 mJ and a peak voltage below 500V.

The positive and negative output terminals of the electric shock simulator were connected to the dorsal side of the subject's left forearm, with the electrodes spaced 5–7 cm apart.

2.2.2. Neutral stimulus

The neutral stimulus employed in this study was a custom-designed cartoon virus pattern, comprising a round green body, two yellow spikes, six green spines, and a pair of large, piercing eyes (Fig. 1A). The dimensions of the green body and yellow spike varied, with their sizes positively correlated with shock probability and subjective pain intensity, respectively.

2.3. Experimental design

This study devised a series of experiments to investigate whether

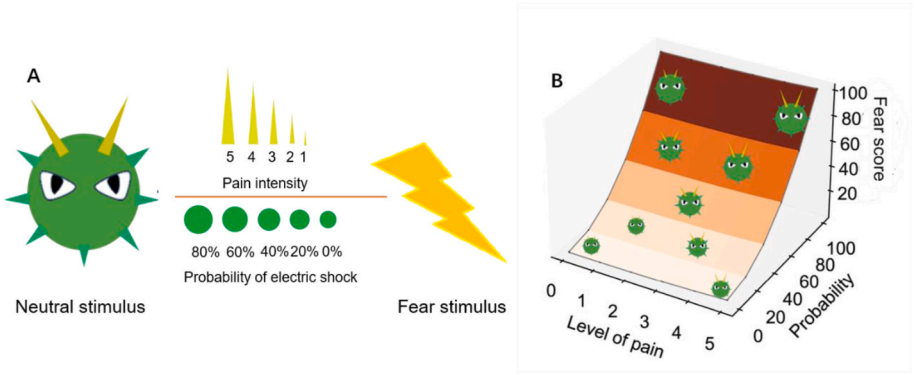

Fig. 1. A schematic view of experimental design for two dimensions of fear space. (A) The custom-generated neutral stimulus images include the spike lengths that associate with subjective pain intensity, as well as the circle sizes that correspond to the probability of a mild electric shock. (**B)** This five-by-five grid represents a two-dimensional fear space which requires to integrate the probability of electric shock and subjective pain intensity into a unified construct. The viral pictures represent learnt cues associated with five different levels of fear intensity and probability, the other ones are unlearnt.

two-dimensional fear learning could construct to a two-dimensional fear system. The study consisted of two primary stages: behavioral training in the morning and fMRI detection in the afternoon. All participants completed the entire experiment within a single day.

In the experimental design, the length of spike (yellow) and the size of the body (green) were varied for neutral cues. The length of spike was positively correlated with pain intensity, while body size was positively correlated with shock probability (see Fig. 1). The two-dimensional fear map was created with coordinates (1, 1), (1, 5), (2, 2), (2, 4), (3, 3), (4, 2), (4, 4), (5, 1), and (5, 5) representing the learned fear-risk categories, while other risk categories were used to detect two-dimensional fear learning.

If individuals successfully form a two-dimensional fear system depicting the relationship between neutral cues and shock risk after effective fear learning, this fear system can be abstractly represented through the following linear model:

$$\textit{Fear score} = \beta_1 \times \text{The length of spike rating} + \beta_2 \times \text{Body size rating} + a$$

Accounting for individual differences, each subject possesses a unique fear response model. According to this model, successful two-dimensional fear learning will exist a fear system to navigate the process.

2.4. Experimental procedure

On the day of the experiment, participants arrived at the laboratory and completed the informed consent process after the experimenter provided an explanation of the experimental procedures and guidelines for MRI scanning.

A crucial variable in this study was subjective pain intensity, categorized into five pain levels, regulated by adjusting voltage intensity. The focus was on the subjective experience of different pain levels rather than the objective intensity of various voltage levels, acknowledging individual differences in the absolute threshold and difference threshold of pain resulting from electric shock. Each participant determined the voltage sequence corresponding to the five pain levels within their maximum pain tolerance range through subjective scoring.

The instrument's voltage range was from a minimum of 15V to a maximum of 100V, with the participants starting at 15V in 5V increments. After each electric shock experience, discomfort ratings ranged from 0 for almost no sensation to 10 for unbearable pain. Participants underwent three rounds of discomfort rating, and the interviewer selected the voltages corresponding to ratings 1, 3, 5, 7, and 9 from the three rounds, averaged to establish the participant's specific voltage sequence. Participants were allowed to stop the experiment at any time if they experienced unbearable pain, although no such instances occurred during the experiment.

Once the specific voltage sequence was determined, participants underwent fear score key training. This score was relevant throughout both the behavioral training and fMRI detection stages, requiring special practice. A horizontal line with a vertical cursor appeared at the top of the screen. Moving left decreased the fear score, while moving right increased it. The leftmost position represented 0, and the rightmost position represented 100, with higher scores indicating higher fear levels. At the start of each score, the cursor appeared at 50 points. Participants pressed ''2'' to move 10 spaces to the left (subtracting 10 points), ''3'' to move 10 spaces to the right (adding 10 points), and ''4'' to confirm the tens digit. Subsequently, they pressed ''2'' or ''3'' to move one space left or right, pressed ''4'' to confirm the single digit, completing a round of fear rating. Participants practiced this process for a total of 20 rounds.

2.5. Experimental task

2.5.1. Neutral cue perception training

During neutral cue size perception training, we categorized the length of the spike and the size of the circle into five levels. Participants were required to accurately distinguish the size level of each circle and the length of the spike. This clarity was essential for the correct assimilation of the relationship between spike length and pain intensity, as well as the relationship between circle size and the probability of electric shock.

The size perception training for circles and spikes unfolded in three distinct stages: the practice stage, the feedback learning stage, and the perception test stage. This sequential approach mirrors the educational process, akin to class instruction, followed by homework, and concluding with an exam. In each stage, circle and spike perception training were conducted separately. Half of the participants underwent circle perception training first, while the other half initiated with angle perception training.

In the practice stage (Fig. 2A), using familiarity with circle size as an example, participants encountered random upward or downward arrows on the computer screen. Upon an upward arrow, a virus stimulus formed by the combination of a fixed-angle third-grade spike and the smallest circle. Conversely, when a downward arrow appeared, the process commenced with the largest circle, gradually decreasing in size. Participants were tasked with memorizing the relationship between the absolute size of each circle unit and its corresponding level. Once they felt sufficiently familiar, they proceeded to the feedback training stage. The spike length perception training followed a similar process as that of circles.

In the feedback training stage (Fig. 2A), taking circle size as an

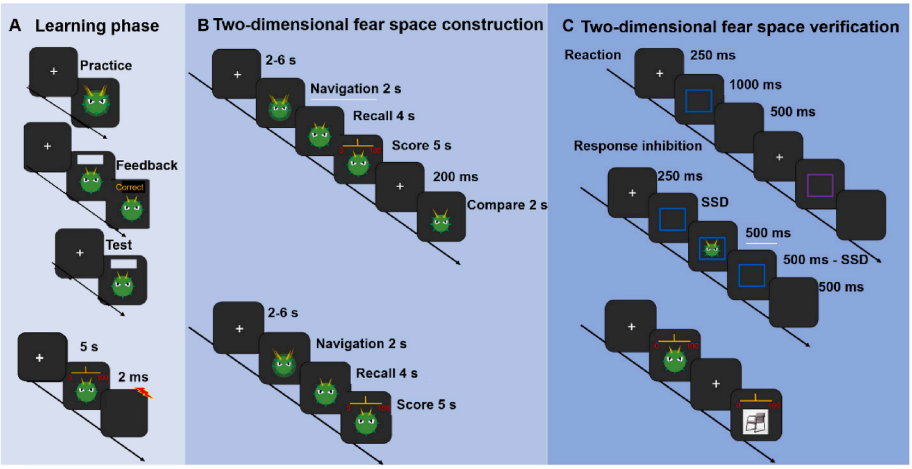

Fig. 2. Experimental procedure diagram. (A) During the learning phase, participants were required to recognize 100% of the viral pictures correctly and to establish a conditioned reflex between the viral pictures and the electric shocks. **(B)** In order to detect the construction of a two-dimensional fear space, participants were required to detect all 25 viral images in the fear space, and actually participants only learned 9 of them. **(C)** Comparison with other neutral pictures verifies that a two-dimensional fear space was indeed constructed, through both implicit and explicit experiments.

example, circles of the five grades appeared three times each, totaling 15 trials. The order of the spikes presented alongside them was no longer fixed but changed randomly. Participants were challenged to remember not based on the absolute size of the circle but by using the length of the unchanged spike as a reference. This intentional complexity aimed to create confusion when both elements changed simultaneously. The process involved a fixation point appearing for the first 200ms on the screen, followed by the random presentation of virus stimuli. Participants were required to input any number from 1 to 5 on the keyboard to indicate the circle level, receiving feedback on correctness. If the overall accuracy rate did not reach 100%, the feedback learning process was repeated until two consecutive 100% correct rates were achieved, allowing entry into the test stage. The diagonal length feedback followed the same procedure as the circle.

The test stage process closely resembled the feedback learning stage (see Fig. 2A), with the only difference being the absence of feedback after each answer. The final correct rate was displayed after 15 trials. The perceptual training concluded when the test phase of each element achieved 100% accuracy twice; otherwise, the test phase continued until the specified requirements were met.

2.5.2. *Two-dimensional fear learning*

Once participants successfully discerned the level of each element, they embarked on fear learning. In a 5x5 grid, encompassing 25 fear scenarios, coordinates (1, 1), (1, 5), (2, 2), (2, 4), (3, 3), (4, 2), (4, 4), (5, 1), (5, 5) were assigned to risk category learning and fear. The spike length of the virus correlated with pain intensity levels 1 through 5, while the body size corresponded to shock probabilities of 0%, 20%, 40%, 60%, and 80%, respectively. The nine risk categories for learning formed an X-shaped pattern on the fear map (Fig. 1B), encompassing the central position and four spikes. This arrangement ensured that subjects could perceive both maximum and minimum risks in the lower left and upper right spikes, facilitating a clear frame of reference for fear scores. The upper left and lower right spikes ensured subjects could distinctly sense the difference between the two dimensions, promoting separation in perception. This design aimed to prevent subjects from learning only pain without considering probability or learning only probability without considering pain. Overall, the selected risk categories for learning covered the entire map.

In the morning, two rounds of fear learning were conducted, each comprising 9 conditions. To maintain equal occurrences of each level of elements, coordinate (3, 3) had 20 trials, while each of the remaining conditions had 10 trials, resulting in a total of 100 trials, with 40 involving shocks of varying strength. The specific process unfolded as follows (Fig. 2A).

First, a 200ms focal point appeared on the screen, followed by a viral stimulus featuring a fear score bar ranging from 0 to 100. Participants were tasked with predicting the risk category of the virus and rating the fear induced by the risk, where 0 denoted no fear and 100 indicated extreme fear. Subsequently, the program administered a shock to the participant based on the actual shock probability and voltage intensity corresponding to the virus stimulus. For instance, if the shock probability was 40%, the participant would receive a level 3 pain electric shock more frequently. The shock probability was pseudo-random. If the probability is 80%, the participant will be shocked 8 times out of 10 trials.

2.5.2.1. Fear navigation tasks. Following fear learning, participants transitioned to detecting fear generalization behavior. The morning fear learning navigation task serves the dual purpose of detecting fear learning and training participants on how to navigate in the fear system, preparing them for the afternoon fMRI detection. The task comprises three sets, each with 72 trials, involving ''fear navigation'', ''fear recall'', ''fear scoring'', and ''fear comparison" stages. The specific process of this task is detailed as follows (Fig. 2B).

First, a fixation point appears on the screen with a jitter of 2–6s, followed by a random virus combination, which may be within the 5x5 map, outside the map, or on/between integer points.

In the fear navigation stage, the virus combination undergoes deformation within 2s, transitioning from one form to another. Starting from a random point on the map, at a specific angle, speed, and displacement distance, the circle and spike change form was determined by the angle and distance. After 2s, the deformation halts, and the final form of the virus remains on the screen for 4s, entering the fear recall stage.

During the 4s of the fear recall stage, participants must recall the entire deformation process of the virus and determine the shape of the virus when it changes for 1s, i.e., the midpoint shape. After 4s, the fear rating stage was initiated.

In the fear rating stage, the final form of the virus remains on the screen for an additional 5s, with the fear score bar appearing at the top. Participants were required to rate the degree of fear induced by the midpoint virus form on a scale of 0–100. The midpoint virus must appear at one of the 5x5 = 25 grid points. After 5s, irrespective of whether the rating was complete or not, the task transitions to the next fixation point. 200ms later, another random virus combination appears, initiating the

fear comparison phase.

In the fear comparison phase, new random virus combinations only emerge at the 5x5 = 25 grid points. 'Participants were tasked with comparing which of the recalled midpoint viruses and the new virus elicited greater sense of fear. If the former, they press the ''2'' key; if the latter, they press the ''3'' key. The newly emerged virus differs by only one element compared to the midpoint virus, allowing for the assessment of participants' accuracy in recalling the midpoint. The fear navigation task serves two purposes, one is to provide a behavioral pre-experiment for the fMRI experiment, and the other is used to analyze the results of the fear learning and generalization phases, which are used to support the creation of a two-dimensional fear space.

2.5.2.2. Fear navigation task: fMRI detection. The fear learning fMRI test was conducted in the afternoon, comprising a total of 4 groups with 72 tests per group. Prior to entering the magnetic resonance imaging (MRI) room, another round of fear learning involving electric shock (e.g., two-dimensional fear learning) was performed to reinstate the fear response to the virus picture. The MRI task closely mirrors the behavioral task (refer to fear generalizes navigation tasks). To streamline the experiment duration during the MRI task, the fear comparison stage was omitted in each trial (refer to Fig. 2B).

2.5.2.3. Emotional stop signal task. Implicit fear detection was conducted using the Emotional Stop Signal Task (Pawliczek et al., 2013; Verbruggen and De Houwer, 2007). In this task, a Go signal was initially presented, prompting the subject to rapidly and accurately press a designated key. However, if a Stop signal appears (No-Go signal) following the Go signal, the subject is required to immediately inhibit the impulse to press the key. Reaction time (RT) is defined as the time elapsed from the appearance of the Go signal to the completion of the key press. Stop signal delay (SSD) refers to the interval between the Go signal and the No-Go signal, representing the delay before the appearance of the No-Go signal. Stop signal response time (SSRT) is the duration it takes for subjects to successfully suppress their keypress impulses after the No-Go signal emerges. If SSD + SSRT < RT, it indicates that the subject successfully inhibited the button press before completion; if SSD + SSRT > RT, it means that the subject did not have sufficient time to suppress the button. Generally, in emotional stop signal tasks, a shorter SSRT suggests higher arousal induced by the No-Go signal.

In this experiment, the Go-to-No-Go trial ratio is set at 3:1, totaling 432 trials. There were three conditions in the No-Go test: a control condition (straw hat picture), a low-risk stimulus (small virus coordinate (1,2)), and a high-risk stimulus (large virus coordinate (5,4)). The viral combinations for low-risk and high-risk stimuli were unlearned during fear learning. The specific experimental process is outlined as follows (Fig. 2C).

During the Go trial, a 250ms fixation point appears on the screen, followed by a Go signal lasting 1000ms. Participants press the ''F" key for a purple rectangle, the ''J" key for a blue rectangle, or allow the screen to automatically transition after 1000ms if no key is needed. A black screen appears for 500ms after 1000ms to conclude the trial.

In the No-Go test, a 250ms fixation point appears on the screen, followed by a Go signal with a dwell time equal to SSD. Subsequently, either the straw-hat image or the virus image appears in the rectangle box, disappearing after 500ms. Following a 500ms-SSD interval, the rectangle transitions to a black screen for 500ms. For each condition in the No-Go trial, SSD is initially set to 250ms, then adjusted by 50ms for each successful suppression and decreased by 50ms for each failed suppression, maintaining a suppression success rate around 50% for each condition.

The emotional stop signal task is performed three times in this study. The first task commences after participant's complete experimental preparation and undergo a round of training, aiming to detect any initial SSRT differences among the three condition groups in the No-Go test before fear learning. The second task initiates after participants complete two rounds of fear learning, assessing whether generalization occurs immediately after fear learning. The third task, conducted after all tasks are completed, aims to test the stability of the fear generalization effect. The emotional stop signal task was used as an implicit experiment to assess whether implicit relationships were established between the neutral stimulus pictures, the small viral pictures, and the large viral pictures in order to verify whether a two-dimensional fear space was constructed.

2.5.2.4. Explicit fear rating task. The explicit fear rating task (Fig. 2C) primarily involves rating 100 images on a scale where 0 denotes no fear at all and 100 represents extreme fear. Fifty of the images were sourced from neutral images in the China Mood Photo Gallery, while the other 50 were selected from combinations of viruses at 5x5 = 25 grid points on the fear map, with each virus appearing twice. The fear rating task was conducted after the initial implicit test and following the final implicit test. By comparing the score changes between the virus group and the control group before and after, as well as examining the score distribution pattern, we can glean insights into fear generalization.

2.6. Data acquisition

2.6.1. Behavioral data acquisition

All behavioral data were gathered using a MATLAB program developed with Psychophysics Toolbox Version 3.

2.6.2. Brain imaging data acquisition

In this study, a Siemens Magnetom Prisma syngo MRD13D (Erlangen, Germany) 3T magnetic resonance scanner equipped with a 64-channel head coil was utilized to acquire T2-weighted, oxygen-dependent brain functional imaging. The scanning parameters were as follows: 48 layers, 3 mm layer thickness, a repetition time (TR) of 3000 ms, echo time (TE) of 30 ms, flip angle (FA) of 90°, voxel size of 3.0 × 3.0 × 3.0 mm^3, and a field of view (FOV) of 210 × 210 mm^2. 341 whole brain (volume) images per run were collected from each participant in the generalization detection task scanning, with a total of 4 runs.

To correct geometric spatial distortion, dual echo-time images covering the entire brain were obtained to create a brain field map. Specific scanning parameters for this process were: TR of 510 ms, TE1 of 4.92 ms, TE2 of 7.38 ms, FA of 60°, voxel size of 3.0 × 3.0 × 3.0 mm^3, and an FOV of 210 × 210 mm^2.

A high-resolution structural image was acquired using a T1-weighted magnetization-prepared rapid gradient echo sequence (MPRAGE). The scanning parameters for this sequence were set as follows: 192 scanning layers, 1 mm layer thickness, TR of 2530 ms, TE of 2.98 ms, FA of 7°, inversion time (TI) of 1100 ms, voxel size of 0.5 x 0.5 x 1.0 mm^2, and an FOV of 256 x 224 mm^3.

Due to the targeted brain regions (EC) being situated at the base of the brain and susceptible to magnetic susceptibility effects, the brain image was tilted 30° in the anterior-posterior (AP) direction before scanning (Deichmann et al., 2003).

2.7. Behavioral data analysis

2.7.1. Fear learning effect analysis

The ability to learn the risk types corresponding to the nine virus forms is crucial for determining the formation of a two-dimensional fear system. The key indicators to assess the effect of fear learning include stability of fear score, fear differentiation, and change in the gap between current fear level and theoretical fear level. During stability of fear score stage, combining the two morning fear learning groups into one, subjects were then categorized into four groups based on the order of learning. Utilizing risk type (9 levels) and the order of learning time period (4 levels) as independent variables and the fear score variance as

the dependent variable, a two-factor repeated measurement ANOVA was conducted. The goal was to investigate whether subjects' fear scores for each risk type tended to become more stable with increased learning times. A smaller variance signifies a more stable score. During fear differentiation stage, combining the two morning fear learning groups into one, subjects were categorized into four groups based on the order of learning. Risk type (9 levels) and the order of learning time period (4 levels) served as independent variables, with the average fear scores as the dependent variable. A two-factor repeated measurement ANOVA was conducted to explore whether, as learning progressed, fear averages for each risk type transitioned from no significant difference to significant difference. Such a shift would indicate an increasing understanding of the risks represented by each virus combination. During change in the gap between current fear level and theoretical fear level stage, derived from the combination of the two morning fear learning groups, the average fear score of the last 5 trials for each risk type was taken as the final score. Each risk category was ranked from low to high based on the average as the standard risk level. The two final scores of each risk category in each trial were then calculated to determine the current risk level. Subsequently, the difference between the current risk level and the final risk level was computed.

2.7.2. Two-dimensional fear space construction analysis

The fear generalization task was designed to confirm that participants had indeed developed a two-dimensional fear system. The prediction bias of the fear response model for the neutral cue fear amount of the learning group after fear learning was not significantly different from that of the generalization group. In essence, this analysis aims to confirm that individuals construct a two-dimensional fear system following risk fear learning, and the fear generalization pattern aligns with this spatial formation. The linear modeling of fear responses is detailed in the supplementary material.

2.7.3. Two-dimensional fear space construction validation analysis

To assess the reality and stability of fear generalization, a comprehensive pre-test and post-test analysis was conducted for both implicit and explicit fear. During implicit fear analysis, a two-factor repeated measurement ANOVA was performed for Stop Signal Reaction Time (SSRT) at 3 detection time points (pre-test vs intermediate test vs post-test) $\times$ 3 No-Go conditions (control condition vs low-risk condition vs high-risk condition). If there is no significant difference in SSRT among the three conditions before and post-fear learning, as well as high-risk conditions being greater than that of low-risk and control conditions, it indicates the occurrence of fear generalization that is accurate and stable. During explicit fear analysis, a two-factor repeated measure ANOVA for fear scores at 2 time points (pre-test vs post-test) $\times$ 2 conditions (virus group vs control group) was conducted. If the fear score in the post-test of the virus group significantly exceeds that in the pre-test, whereas no significant difference between the pre-test and post-test of the control group, it suggests the presence of fear generalization. A three-factor repeated measurement ANOVA was perfomred based on the fear score of 5 spike lengths $\times$ 5 circle sizes $\times$ 2 time points (pre-test vs post-test). If the fear score shows no correlation with spike length and circle size in the pre-test, but a positive correlation emerges in the post-test where larger spikes or circles lead to higher fear scores, it signifies the presence of accurate and correct generalization. The prediction bias of the neutral cue fear amount of the learning group before fear learning was significantly greater than that of the learning group after fear learning, indicating an absence of a floor effect.

2.8. Brain imaging data analysis

2.8.1. MRI data preprocessing

During the initial scanning stage, the magnetic resonance signal requires time to achieve basic stability. Thus, FSL software was employed to discard the first two volumes of the functional data for each run, totaling 6 s of time series. Then, the functional volumes undergo preprocessing via fMRIPrep (Esteban et al., 2019)—a globally recognized and standardized brain data preprocessing workflow, encompassing the following steps. In artifact removal stage, the steep spikes or slow drifts were identified and removed. Slice timing was performed to interpolate data at the same time point between brain slices to reconstruct a synchronized 3D brain image. Realignment accounting for spatial translation and rotation between each volume spatially aligns all other volumes with the first volume in the time series. The brain field map derived from dual echo-time images covering the entire brain was employed to rectify geometric spatial distortions. The mean brain functionl volumes were co-registered to the high-resolution T1-weighted structural image corresponding to each subject through linear transformation, which was followed by the normalization into a common standard spatial template (Montreal Neurological Institute (MNI)). Finally, the data undergoes smoothing using the SPM (Statistical Parametric Mapping) tool based on MATLAB, with an isotropic three-dimensional Gaussian kernel (full-width at half-maximum set to 6 mm).

2.8.2. Whole brain univariate analysis

All whole-brain univariate analyses were executed using SPM12 in MATLAB. Following pre-processing, we modeled the fMRI time series utilizing a Generalized Linear Model (GLM). To explore brain activity during the fear navigation task, we categorized it into three conditions: ''fear navigation", ''fear recall", and ''fear scoring", considering the differences in cognitive engagements. For the 4s fear recall, only the second 2s were chosen for regression modeling, excluding cases with excessive fear navigation activities in the initial 2s. In order to exclude the effect of the fear recall phase, the fear scoring phase consisted of 5s excluding the first 2s and selecting only the last 3s for regression modeling. Due to the ongoing development of fear recall and fear assessment, it was challenging to directly distinguish between the processes involved in these two phases. Thus, to inspect the evaluation processing towards learned fear stimuli, the contrast analysis was conducted between fear scoring phase and fear navigation phase, the former of which was strongly affected by fear navigation through recalling. A generalized linear model was constructed with three conditions and six columns of head motion parameters as regressors. All terms were convolved with the FSL default hemodynamic response function and subjected to high-pass filtering with a 1/128 Hz cut-off point before entering GLM. In this study, the implicit threshold used during model estimation at the individual analysis stage was replaced with an explicit mask in the default path of SPM12 (the "mask_ICV.nii" file). This change was made based on our observation that using the implicit threshold might result in signal loss in the entorhinal region and frontal region. Drawing upon previous literature, we opted for the explicit template as it was deemed a more reliable choice (Ruge et al., 2019). Subsequently, group analysis was conducted based on the aforementioned model analysis. We conducted a whole-brain analysis of the following 4 phases fear navigation phase, fear recall phase, fear recall over fear scoring phase, and fear scoring over fear recall phase. The fear navigation phase and the fear recall phase perform different tasks, and we need to detect brain activation while performing the different tasks. For corretion of false positive introduced by multiple comparisons, the FDR method was employed to correct the p-value of the *t*-test (pFDR <0.05).

3. Results

3.1. Behavioral results

3.1.1. Fear learning effect

During fear stability stage, participants undergoing two-dimensional fear learning in the morning were segmented into four learning periods based on the learning order. A two-factor repeated measurement ANOVA was conducted, utilizing risk category (9 levels) and the order of

the learning period (4 levels) as independent variables and the variance of the fear score as the dependent variable. The results are summarized in Fig. 3A.

The main effect of the learning time period was significant (F (3,63) = 5.38, p = 0.002). The variance during the first time period was significantly higher than that of the second time period (t (21) = 2.56, p = 0.018), and the fourth time period (t (21) = 3.57, p = 0.002). Additionally, the main effect of risk categories was significant (F (8,168) = 2.24, p = 0.027).

As depicted in Fig. 3A, with increasing fear learning sessions, the mean variance of subjects' fear scores generally decreases. Concurrently, the standard error diminishes, indicating an overall enhancement in the stability of subjects. In simpler terms, subjects with relatively stable scores exhibited increased stability with more learning sessions, while those with initially unstable scores gradually achieved stability over time.

Regarding risk categories, excluding two risk categories with the highest pain index, grade 5 pain - grade 5 probability, and grade 5 pain - grade 1 probability, which experienced an abnormal increase in the third learning period, each risk combination level demonstrated a trend of stability with increased learning sessions. The abnormalities in the variance of the fear score for the two risk combination levels in the third learning period, pain intensity level 5 and probability of electric shock level 5, and pain intensity level 5 and probability of electric shock level 1, was likely attributed to the fact that the subjects took a break after completing the first set of fear learning. Upon resuming the second set of fear learning, subjects with a relax during the break became highly apprehensive about pain intensity level 5, leading to a more noteworthy response in some individuals. Consequently, both the total variance and the standard error of variance were higher than those in the second learning period.

During fear differentiation stage, the two groups of morning fear learning were consolidated into one group, subsequently segmented into four learning periods based on the order of learning. Risk category (9 levels) and the order of learning periods (4 levels) were considered as the independent variables, and the average fear score was used as the dependent variable. The outcomes of the two-factor repeated measurement ANOVA were depicted in Fig. 3B. The main effect of risk categories was significant (F (6, 168) = 65.63, $p < 0.001$). The results of the multi-comparison analysis are shown as follows. The pain intensity level 5 and probability of electric shock level 5 was significantly higher than that of every other risk category ($p < 0.001$). The pain intensity level 5 and probability of electric shock level 1 was significantly higher than pain intensity level 2 and probability of electric shock level 4 ($p < 0.001$), pain intensity level 2 and probability of electric shock level 2 ($p < 0.001$), pain intensity level 1 and probability of electric shock level 5 ($p < 0.001$), and pain intensity level 1 and probability of electric shock level 1 ($p < 0.001$). The pain intensity level 4 and probability of electric shock level 4 was significantly higher than pain intensity level 3 and probability of electric shock level 3 ($p < 0.005$), pain intensity level 2 and probability of electric shock level 4 ($p < 0.001$), pain intensity level 2 and probability of electric shock level 2 ($p < 0.001$), pain intensity level 1 and probability of electric shock level 5, and pain intensity level 1 and probability of electric shock level 1 ($p < 0.001$). The pain intensity level 4 and probability of electric shock level 2 was significantly higher than pain intensity level 2 and probability of electric shock level 4 ($p < 0.005$), pain intensity level 2 and probability of electric shock level 2 ($p < 0.001$), pain intensity level 1 and probability of electric shock level 5 ($p < 0.001$), and pain intensity level 1 and probability of electric shock level 1 (<0.001). The pain intensity level 3 and probability of electric shock level 3 was significantly higher than pain intensity level 2 and probability of electric shock level 2 ($p < 0.001$), pain intensity level 1 and probability of electric shock level 5 ($p < 0.001$), and pain intensity level 1 and probability of electric shock level 1 ($p < 0.001$). The pain intensity level 2 and probability of electric shock level 4 was significantly higher than pain intensity level 1 and probability of electric shock level 5 ($p < 0.031$) and pain intensity level 1 and probability of electric shock level 1 ($p < 0.001$). The pain intensity level 2 and probability of electric shock level 2 was significantly higher than pain intensity level 1 and probability of electric shock level 1 ($p < 0.001$). The pain intensity level 1 and probability of electric shock level 5 higher than pain intensity level 1 and probability of electric shock level 1 ($p < 0.001$). In essence, participants were adept at distinguishing the risk content represented by various viral stimuli.

Furthermore, the main effect of the learning period was significant (F (3, 63) = 4.34, p = 0.008). The average fear score during the first learning period was notably lower than that of the second learning period (t (63) = −2.7, p = 0.009), and the third learning period (t (63) = −2.043, p = 0.045), and the fourth learning period (t (63) = −3.42, p = 0.001). This suggests that as the number of fear learning sessions increased, the perceived fear by subjects progressively heightened. The efficacy of fear learning transitioned from abstractly estimating risk to realistically perceiving it.

A noteworthy observation was that in the initial learning period, the average fear scores for different risk combinations already exhibited distinctions. This phenomenon may stem from subjects being pre-informed that the length of the virus spike is related to the pain level, and the virus size corresponds to the probability of electric shock. Consequently, subjects easily inferred that longer spike implied higher pain levels and larger bodies indicated a greater probability of electric

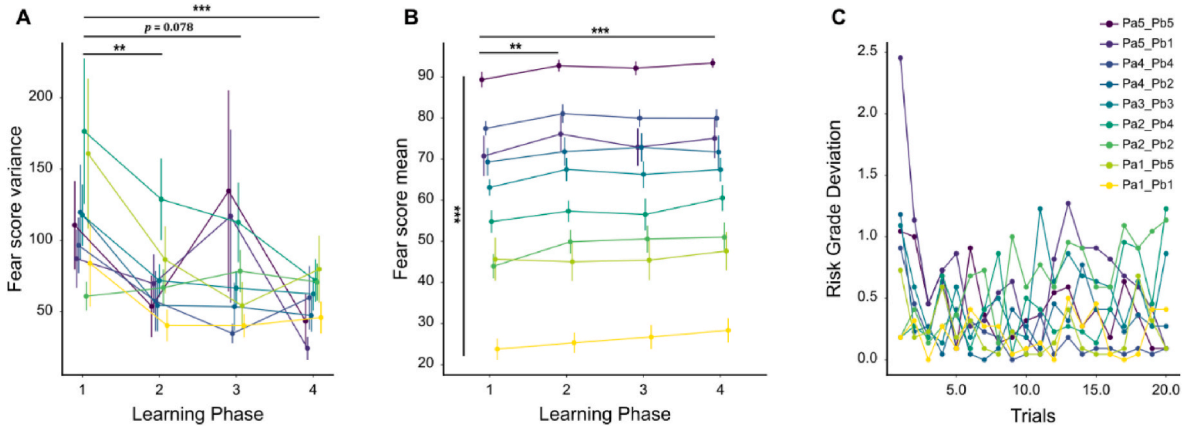

Fig. 3. Fear learning effect. (A) Fear stability found that as the number of fear learnings increased participants' fear score variance decreased and fear score stability increased. **(B)** Fear differentiation found that participants could distinguish the meaning of different viral pictures. **(C)** As the number of trials increased, the difference between participants' current and theoretical fear ratings was decreasing, indicating that fear learning was effective. ''Pa'' represents pain intensity level 1 to 5, and ''Pb'' represents probability of electric shock 0–80%.

shock. This preliminary estimation at the outset could hinder the subjects' exploration and learning, indicating that providing this information might impede the subjects' unbiased learning experience. As depicted in Fig. 3C, the diminishing gap between the group's risk levels with the increase in learning sessions implies the effectiveness of our two-dimensional fear learning. In fact, we also attempted to accomplish both processes through implicit learning during the pre-experiment, but this undoubtedly greatly increased the difficulty of the experiment, resulting in a large percentage of subjects being unable to complete the experiment. However, the integration of the two was accomplished through implicit learning.

3.1.2. Two-dimensional fear space construction

To validate those subjects indeed formed a two-dimensional fear map and successfully generalized their fear responses, we divided each set of two-dimensional fear navigation tasks into four stages. The degree of fear induced by virus stimulation was then compared with the theoretical fear (as illustrated in Fig. 4A).

As depicted in Fig. 4A, from the initiation of the first stage in the initial set of fear navigation tasks, there was no significant difference in the degree of fear induced by the virus stimulus compared to the theoretical degree of fear between the learning and generalization conditions. Based on the linear modeling of fear responses, the theoretical degree of fear was derived from the values of a, values β1 and β2 on table s1 for each subject, as well as corresponding the lengths of the spikes and the body size rating (Fig. 1B). This pattern persisted in each subsequent stage. These findings strongly indicate that subjects establish a two-dimensional fear system post-learning risk fear, and the fear generalization pattern adheres to this spatial framework.

3.1.3. Two-dimensional fear space construction validation

To assess the reality and stability of fear generalization, we conducted pre- and post-test analyses for both implicit and explicit fear. For the implicit Emotional Stop Signal Task, we performed a two-factor repeated-measurement ANOVA of SSRT with three detection time points (pre-test vs The mid-test is the second task vs post-test) and three No-Go conditions (control condition vs low-risk condition vs high-risk condition). The results are presented in Fig. 4B. The main effect at the detection time point was significant ($F(2,18) = 6.39$, $p = 0.008$), with SSRT at the pre-test significantly higher than at the mid-test (t (18) =

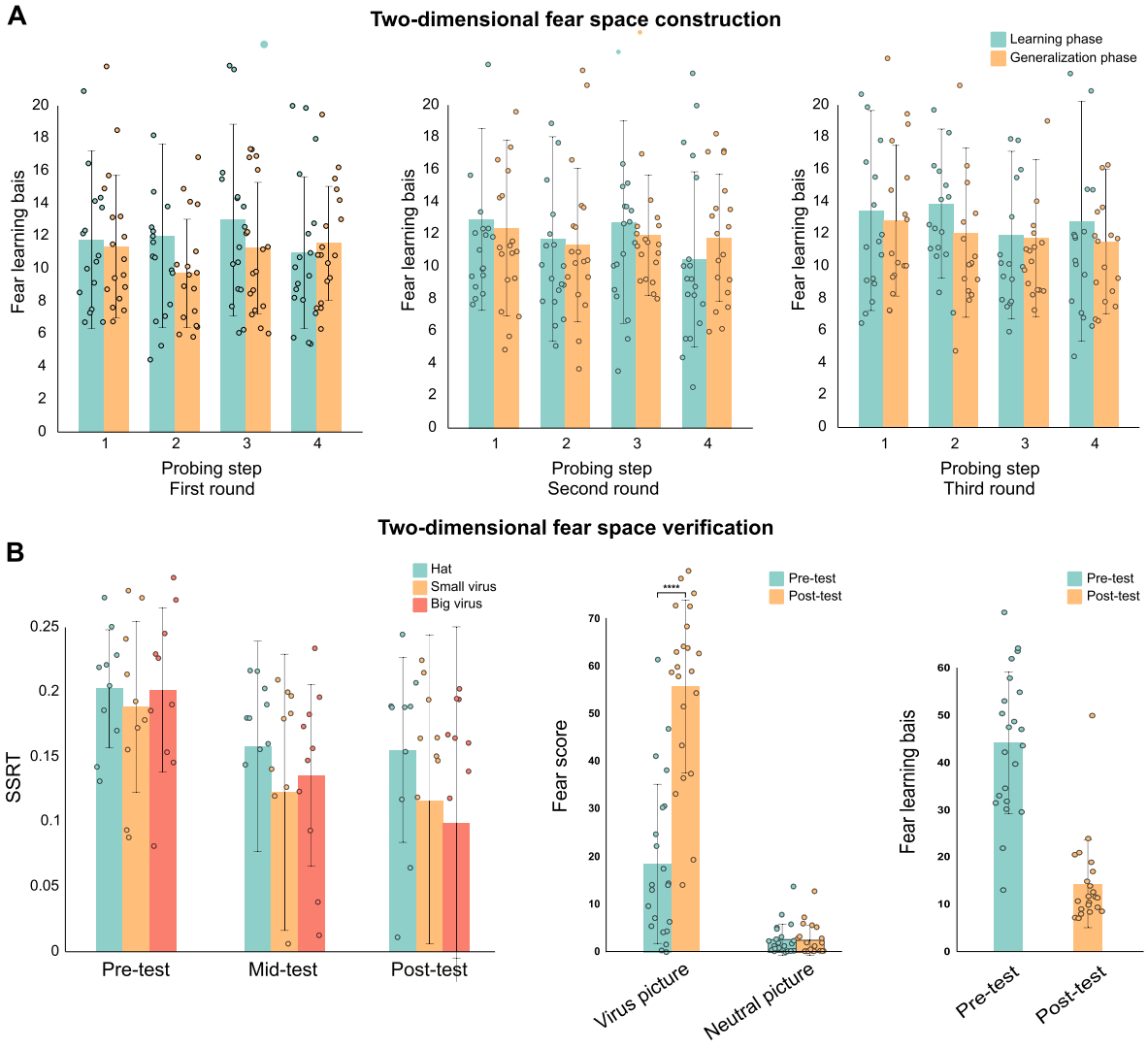

Fig. 4. Two-dimensional fear system verification. (A) Three groups of fear navigation tasks found that the difference between the theoretical and actual values of the two conditions did not have a significant gap at each stage. **(B)** This phase focuses on validating the construction of a two-dimensional fear space through implicit and explicit tasks. The results of the SSRT task showed the shortest reaction time for large viruses followed by small viruses and hat picture. Pre-test and post-test analyses for the explicit fear rating task revealed that the unlearned viral picture fear ratings were significantly higher on the post-test than on the pre-test. We found that the difference between the theoretical and actual values of the posttest was much less than that of the pretest, and that there was no floor effect.

2.68, $p = 0.039$) and the post-test (t (18) = 3.39, $p = 0.009$). As depicted in Fig. 4B, no significant differences in SSRT were observed among the three conditions before two-dimensional fear learning. Following fear learning, SSRT in the risk condition started to decrease compared to the control condition. At the experiment's conclusion, SSRT remained unchanged in the control group, while SSRT in the high-risk condition significantly decreased. These findings indicate the occurrence of fear generalization, demonstrating a correct and stable generalization pattern. The main effect of the detection time point was significant (F (1, 21) = 103, $p < 0.001$), the main effect of the group was significant (F (1, 21) = 124, $p < 0.001$), and the interaction between the detection time point and the group was significant (F (1, 21) = 102, $p < 0.001$).

As observed in Fig. 4B, the fear score in the virus group post-test was significantly higher than in the pre-test (t (42) = −14.35, $p < 0.001$), while no significant difference was noted in the control group before and after the test, indicating the presence of fear generalization. To ensure that any observed differences between theoretical and actual fear values in the two-dimensional fear navigation task weren't merely due to a floor effect, we compared whether significant differences existed between the theoretical and actual fear values in the pre-test explicit fear scoring task and the two-dimensional fear navigation task. Fig. 4B illustrates that the difference between the theoretical and actual values of post-test explicit fear scores was significantly lower than that of the pre-test (t (21) = 8.43, p < 0.001), indicating that the disparity between theoretical and actual fear values was approximately 10, ruling out the possibility of a floor effect. Subjects indeed established a consistent set of standards for perceiving the fear induced by virus stimuli.

3.2. Whole brain univariate results

During the fear navigation phase, we endeavored to localize brain areas tracking the dimensional changes within learned fear space. This analysis revealed significant activation in core regions of three large-scale functional networks: 1) the emotional salience network including the bilateral insula, the left ACC, middle cingulate cortex, as well as the hippocampus, parahippocampal gyrus, and the amgydala, 2) the sensorimotor network including the middle occipital and superior occipital gyrus, fusiform gyrus, precentral gyrus, supplementary motor area and supramarginal gyrus, 3) the frontal-parietal network including the inferior parietal lobule, superior parietal lobule, dlPFC, middle frontal gyrus, inferior temporal gyrus (t (22) > 2.87, $p < 0.05$ FDR corrected) (see Table 1). In the ''fear recall" phase, significant activation occurred in the bilateral ACC, amygdala, middle frontal gyrus, hippocampus, insula, inferior occipital gyrus, and the left dlPFC, superior frontal gyrus, and the right inferior frontal gyrus, lingual gyrus (t (22) > 2.51, $p < 0.05$ FDR corrected). The activation during the ''fear scoring" phase highly mirrored those in the ''fear recall" phase, except the right of red nucleus (t (22) > 2.31, $p < 0.05$ FDR corrected) (Fig. 5C). To indirectly inspect the evaluation process for learned fear stimuli, we conducted a whole-brain contrast of fear scoring over fear navigation, in order to exclude the effects of the fear navigation stage which strongly affect fear evaluation through recalling. Such analysis revealed the activations within crucial regions of cognitive evaluation, including the bilateral amygdala, ACC, dlPFC, insula, and the right parahippocampal (t (22) > 2.58, $p < 0.05$ FDR). Additionally, the significant activations of bilateral amygdala extending to hippocampus were also observed, which maybe indicate the contribution of emotional memory formed during fear learning. Bilateral middle frontal gyrus, superior frontal gyrus, postcentral gyrus, and the left medial frontal gyrus, orbital gyrus, pons, and the right middle cingulate cortex, inferior occipital gyrus, and supramarginal gyrus (t (22) > 2.58, $p < 0.05$ FDR) were also activated. Whole brain activation was progressively increased from the fear navigation stage, the fear recall stage to the fear scoring stage.

Table 1
Whole brain activation for the fMRI experiment.

Contrast	Region (AAL label)	L/R	T	MNI (x y z)	K (voxel)
Fear Navigation Phase					
	Lingual_R (aal3v1)	R	8.61	22 -86 -6	10382
	Occipital_Inf_R (aal3v1)	R	8.54	44 -74 -4	
	Temporal_Inf_R (aal3v1)	R	8.18	50 -62 -4	
	Fusiform_L (aal3v1)	L	8.52	−22 -86 -10	6697
	Occipital_Mid_L (aal3v1)	L	9.08	−32 -80 2	
	Occipital_Sup_L (aal3v1)	L	7.69	−16 -94 8	
	Occipital_Sup_L (aal3v1)	L	4.97	−24 -80 34	2840
	Parietal_Inf_L (aal3v1)	L	6.12	−44 -46 44	
	Parietal_Sup_L (aal3v1)	L	5.59	−18 -72 42	
	Frontal_Inf_Oper_L (aal3v1)	L	4.38	−44 12 8	776
	Precentral_L (aal3v1)	L	4.88	−48 0 24	
	Precentral_R (aal3v1)	R	5.34	50 4 26	
	Sub-Gyral	R	4.56	44 10 16	
	Cingulate_Mid_L (aal3v1)	L	5.59	−8 22 38	667
	Supp_Motor_Area_L (aal3v1)	L	4.68	−8 14 52	
	Supp_Motor_Area_R (aal3v1)	R	4.9	10 18 46	
	Insula_L (aal3v1)	L	4.42	−36 20 0	397
	Insula_L (aal3v1)	L	4.93	−28 18 12	
	Frontal_Inf_Tri_L (aal3v1)	L	5.41	−34 28 8	
	Thal_LGN_R (aal3v1)	R	7.55	20 -28 0	321
	Thal_LGN_L (aal3v1)	L	6.86	−22 -28 -4	253
	Thal_PuM_L (aal3v1)	L	3.67	−10 -30 0	
	Cerebellum_Crus2_R (aal3v1)	R	5.01	26 -74 -44	240
	Frontal_Sup_2_L (aal3v1)	L	4.58	−22 0 48	197
	Frontal_Sup_2_L (aal3v1)	L	5.6	−18 20 64	186
	Frontal_Inf_Tri_R (aal3v1)	R	3.54	48 32 18	131
	Frontal_Mid_2_R (aal3v1)	R	3.71	50 4 56	86
	Anterior Cingulate Cortex	L	4.29	−8 22 42	72
	Paracentral_Lobule_R (aal3v1)	R	4.26	8 -28 64	70
	Parahippocampa Gyrus	R	5.24	18 -32 -4	66
	Temporal_Pole_Mid_L (aal3v1)	L	3.84	−28 8 -38	38
	Parahippocampa Gyrus	L	4.6	−18 -32 -4	37
	Insula_R (aal3v1)	R	3.56	38 -2 10	35
	dl PFC	R	3.41	4 16 44	34
Fear Recall Phase					
	Lingual_R (aal3v1)	R	11.55	18 -84 -6	52625
	Occipital_Inf_L (aal3v1)	L	12.44	−28 -82 -2	
	Occipital_Inf_R (aal3v1)	R	11.39	42 -78 -8	
	Frontal_Inf_Oper_R (aal3v1)	R	5.82	58 8 22	1425
	Insula_R (aal3v1)	R	4.49	40 4 4	
	Insula_L (aal3v1)	L	3.49	−40 5 -2	907
	Frontal_Mid_2_L (aal3v1)	L	3.84	−34 42 8	315
	Frontal_Sup_2_L (aal3v1)	L	4.57	−32 56 22	
	Amygdala	L	5.07	−16 -4 -6	149
	Amygdala	R	3.29	16 -8 -8	123
	Frontal_Inf_Tri_R (aal3v1)	R	2.64	42 34 24	85
	Frontal_Mid_2_R (aal3v1)	R	3.45	46 38 36	
	Hippocampus_L (aal3v1)	L	5.67	−20 -30 -6	65
	Hippocampus_R (aal3v1)	R	5.76	24 -31 -6	61
	ACC_sup_R (aal3v1)	R	4.57	10 22 28	57
	ACC_sup_L (aal3v1)	L	3.93	−10 22 30	42
	dl PFC	L	2.61	−10 26 28	
Fear Scoring Phase					
	Occipital_Inf_R (aal3v1)	R	10.05	32 -92 -6	83869
	Red_N_R (aal3v1)	R	9.61	8 -20 -14	
	Insula_L (aal3v1)	L	5.02	−34 14 0	1274
	Frontal_Mid_2_R (aal3v1)	R	5.14	34 42 26	1078
	dl PFC	R	4.75	8 22 38	916
	dl PFC	L	4.62	−10 22 38	811
	Insula_R (aal3v1)	R	4.42	44 13 0	665

(continued on next page)

Table 1 (*continued*)

Contrast	Region (AAL label)	L/R	T	MNI (x y z)	K (voxel)
	ACC_sup_L (aal3v1)	L	3.39	−6 18 25	357
	ACC_sup_R (aal3v1)	R	3.57	10 18 25	273
	Hippocampus_L (aal3v1)	L	4.06	−24 -36 0	170
	Calcarine_R (aal3v1)	R	2.94	14 -70 14	123
	Hippocampus_R (aal3v1)	R	5.21	20 -34 0	119
	Frontal_Mid_2_L (aal3v1)	L	2.85	−40 26 34	78
	OFCant_L (aal3v1)	L	4.33	−20 42 -12	43
	Amygdala_L (aal3v1)	L	4.03	−24 -4 -13	30
Fear Scoring Phase > Fear Navigation Phase					
	Medial Frontal Gyrus	L	6.49	−8 -14 74	43477
	Postcentral_L (aal3v1)	L	7.36	−30 -30 72	
	Frontal_Mid_2_R (aal3v1)	R	5.3	36 52 20	1437
	Frontal_Sup_2_R (aal3v1)	R	4.65	26 30 30	
	Insula_L (aal3v1)	L	4.15	−42 12 -6	995
	Insula_R (aal3v1)	R	5.74	48 -12 -6	808
	SupraMarginal_R (aal3v1)	R	5	60 -20 24	778
	dl PFC	R	4.21	8 22 30	774
	Anterior Cingulate Cortex	R	3.53	11 34 18	429
	Anterior Cingulate Cortex	L	3.15	−10 34 18	425
	dl PFC	L	2.84	−8 28 30	
	OFCant_L (aal3v1)	L	5.34	−22 48 -16	309
	OFCmed_L (aal3v1)	L	3.07	−10 54 -24	
	Superior Frontal Gyrus	L	4.74	−20 58 -18	
	Frontal_Sup_2_R (aal3v1)	R	2.99	26 52 -6	295
	OFCant_R (aal3v1)	R	6.12	28 60 -16	
	OFCmed_R (aal3v1)	R	3.5	20 40 -18	
	Frontal_Mid_2_L (aal3v1)	L	3.88	−36 48 24	250
	Orbital Gyrus	L	3.71	−8 44 -32	188
	Superior Frontal Gyrus	R	3.59	8 60 -26	
	Cingulate_Mid_R (aal3v1)	R	3.65	10 -36 46	169
	Occipital_Inf_R (aal3v1)	R	5.01	32 -96 -8	164
	Medulla	L	3.51	0 -30 -46	162
	Pons	L	2.96	−8 -32 -40	
	Postcentral_R (aal3v1)	R	4.09	50 -32 60	74
	ParaHippocampal_R (aal3v1)	R	2.99	16 -40 -10	57
	Amygdala_L (aal3v1)	L	3.83	−20 0 -13	29

Note: L, left cerebrum; R, right cerebrum; dl PFC, dorsolateral prefrontal cortex.

4. Discussion

This study used an innovative paradigm with two-dimensional fear space design and surpassed traditional one-dimensional fear learning approaches. Behaviorally, participants successfully constructed a fear space though the learned relations at the diagonal of a 5*5 two-dimensional grid to entire space. Analysis of fMRI data during construction and navigation within a two-dimensional fear space revealed functional engagement in widespread regions of large-scale brain networks, including the emotional salience network (i.e., the amygdala, insula, ACC), memory-related regions (i.e., the hippocampus and parahippocampal gyrus extending into the entorhinal cortex), as well as the frontal-parietal network (.e., the dlPFC and posterior parietal cortex).

For behavioral results, participants successfully differentiated and consistently evaluated the fear scores of the 9 viral stimuli, demonstrating a stable association constructed between fear responses and two dimensions of viral stimuli. The head spike and body size of virus, representing probability and intensity of electric shocks, appeared together with fear scores before the conditioning procedure, and participants acquired the joint effect on fear scores likely by relational reasoning. This was mirrored through linear modeling the relation between levels of actual fear score and individual's rating. Moreover, the probability and intensity of shock collectively contributed to enhance the fear acquisition to virus through the classical associative learning (Lissek et al., 2014; McNally and Westbrook, 2006; Mitchell et al., 2009). And the linear modeling of fear scores also effectively predicted the degree of fear for both the learned and unseen viruses. Together, our behavioral findings confirm the existence of a two-dimensional fear space. Meantime, results from fear navigation tasks showed no significant differences between theoretical and actual fear scores, suggesting the successful construction and also the utilization of the two-dimensional fear system. This receives additional support from results of the implicit and explicit experiments. In the implicit emotional stop signal task, larger viral pictures with higher fear scores showed significantly faster responses after fear learning compared to smaller ones with lower scores. In the explicit fear scoring task, viral pictures scored significantly higher than neutral pictures post-learning, with no change in scores for neutral pictures before and after learning. It was noteworthy that the difference between the theoretical and actual fear scores of viral pictures before fear learning was significantly greater than after fear learning through further validation, therefore there was no floor effect.

For fMRI findings, activation of the hippocampus, parahippocampal gyrus, insula, anterior cingulate gyrus, and dlPFC were observed in each stage, and activation of the amygdala was added to the phases of fear recall, fear score, and fear score over fear navigation. During the navigation phase, continuously changing fear pictures have been brought to the attention of the dlPFC, and memory was extracted through the parahippocampal gyrus, amplifying the signal with functional involvement of the insula and ACC, core regions of the salience network (Menon and Uddin, 2010; Palaniyappan and Liddle, 2012; Schimmelpfennig et al., 2023; Seeley, 2019). The amygdala, hippocampal and parahippocampal gyrus was activated during the fear recall phase, which points out the contributions of memory formed during learning the link between the combination of dimensions and fear (Alvarez et al., 2008; Hermans et al., 2017). Alternatively, the intensity and probability of shocks are possibly encoded in the emotional and salience networks, and collectively contributes to fearful ratings, which also receives supports from activation of the amygdala extending to EC derived from fear scoring phase. The bilateral dlPFC as well as EC activation during the fear scores might suggests that fear evaluation requires more attention and possible top-down regulation of reactive expression for emotional stimuli (Baldi and Bucherelli, 2014; Brosnan and Wiegand, 2017; Coutureau and Di Scala, 2009; Eippert et al., 2007; Kluen et al., 2019; Roesler and McGaugh, 2022; Takehara, 2014; White et al., 2023). In brief, the neural mechanisms underlying the construction of a two-dimensional fear space involve the emotional salience network, including the amygdala, insula, ACC, and dlPFC, as well as regions responsible for memory including the hippocampus and parahippocampal gyrus extending into the EC.

To summarize, the amygdala, hippocampus, anterior insula, ACC, and dlPFC collectively and dominantly contribute to the construction of two-dimensional fear space. These regions play crucial roles in processing and integrating information across multiple brain areas (Dolcos et al., 2011; Jung et al., 2022; Šimić et al., 2021; Zhao et al., 2023), especially in the context of emotional processing and memory formation. The AI, ACC, and dlPFC have intricate connections with the amygdala (Berboth and Morawetz, 2021; Bissière et al., 2008; Höistad and Barbas, 2008), serving as pivotal nodes for emotional processing. These areas are essential for detecting and processing emotional salience (Ince et al., 2023; Luo et al., 2014; Menon and Uddin, 2010; Seeley, 2019), thereby facilitating fear learning and generalization. The AI and ACC, as part of the salience network (Menon and Uddin, 2010; Seeley, 2019), are specifically responsible for identifying emotionally significant stimuli and preparing the brain to respond to these stimuli (Luo et al., 2014). This response involves coordinating with the amygdala, which processes threats from the external environment and helps establish conditioned reflexes between such threats (like electric shocks) and associated stimuli (like viral pictures). Furthermore, the relationship between the AI, ACC, dlPFC, and the hippocampus underscores the

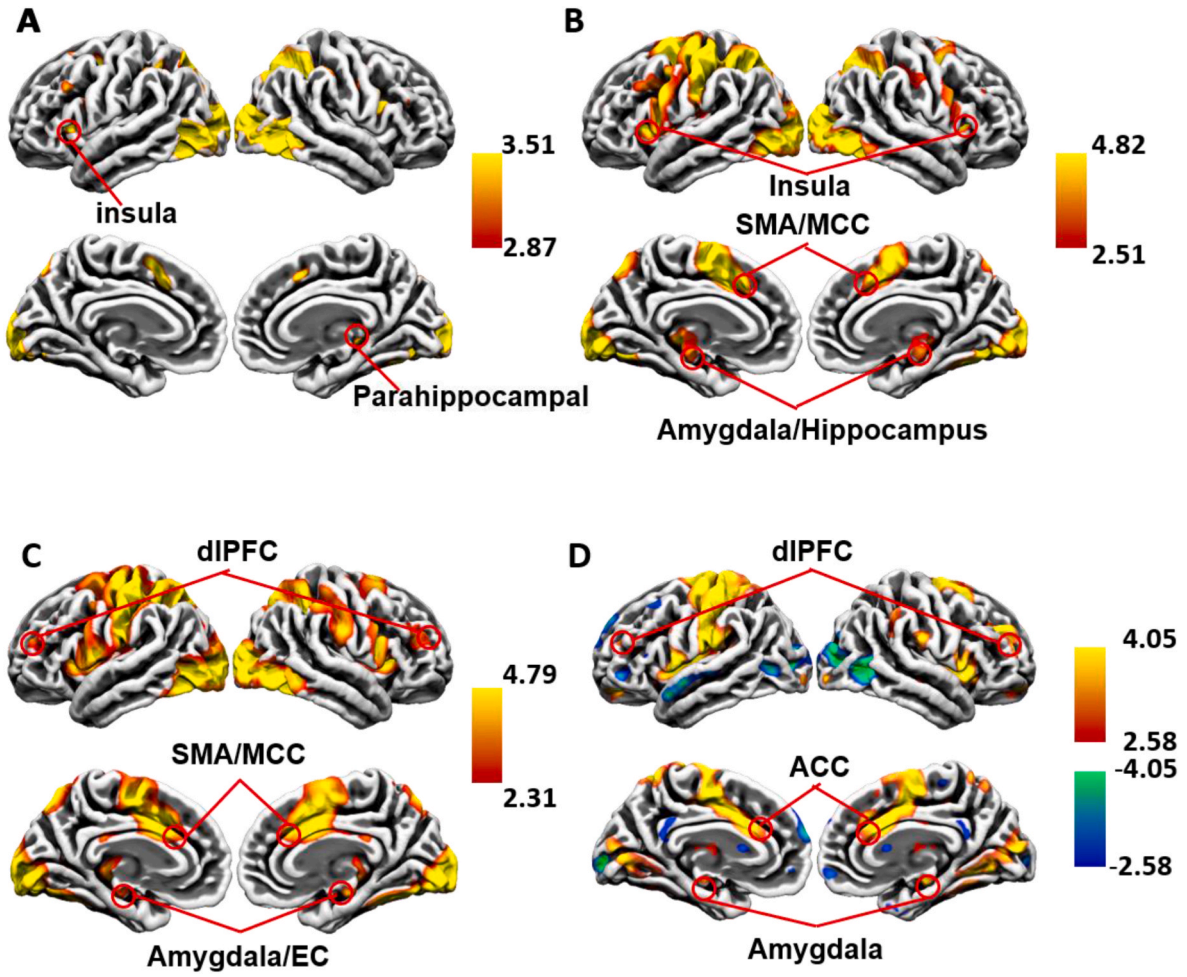

Fig. 5. Whole Brain Activation Intensity. **(A)** Activation of the left parahippocampal gyrus during the fear navigation phase. **(B)** Bilateral activation in supplementary areas, occipital cortex, and insula during the fear recall phase. **(C)** Activation similar to the fear recall phase is in the fear scoring phase. **(D)** Regions demonstrate significant distinctions in activations between the fear scoring phase (autumn) and the fear navigation phase (winter). MCC: middle cingulate cortex, SMA: supplementary motor area, ACC: anterior cingulate cortex, dlPFC: dorsal lateral prefrontal cortex, EC: entorhinal cortex.

integration of emotional processing with memory systems (Dolcos et al., 2011; LaBar and Cabeza, 2006). The hippocampus, particularly its dorsal region, is crucial for processing situational memory related to fear (Anagnostaras et al., 2001; Chaaya et al., 2018), working closely with the amygdala to maintain and consolidate these fear memories (Chaaya et al., 2018). The dlPFC contributes to this network by regulating attention towards fear-relevant stimuli and modulating emotional responses through top-down control (White et al., 2023; Kroes et al., 2019; Vogt, 2019; Vuilleumier et al., 2003), thus influencing how fear memories are formed and retrieved. Thus, the emotional salience network, comprising the AI, ACC, amygdala and hippocampus, along with regions in the frontal-parietal network, forms a complex system that not only processes and regulates emotional and fear responses, but also plays a critical role in the encoding and retrieval of fear-related memories (Liu et al., 2016; Zhuang et al., 2022). This network's ability to integrate information from various brain regions enhances our understanding of the construction of the two-dimensional fear space, highlighting the interconnectedness of emotional and memory processes in the human brain.

4.1. Limitations and future studies

Despite the valuable insights gained from our study, several limitations warrant consideration, and these areas should be addressed in future study designs. Firstly, our current task design lacks of a reinforcement learning manipulation, preventing a comprehensive analysis of the entire learning process during data analysis. Linear modeling of learning results was currently limited to regression analysis, resulting in the loss of significant learning information. Future endeavors should incorporate a reinforcement learning paradigm and leverage machine learning methods for a more nuanced analysis (Bălan et al., 2019; Petrescu et al., 2021). Secondly, the absence of physiological indicators of fear, such as pupillary recording and skin electromyography (Kret et al., 2013), limits the depth of fear detection analysis. In subsequent studies, including these physiological indicators will provide a more comprehensive understanding of fear responses. Thirdly, our assertion that the learning of risk-based fear was rooted in individuals subjectively constructing a quantitative relationship between neutral cues and real risks aligns with the Bayesian brain theory in cognitive neuroscience. The brain constantly models input information to enhance prediction and reasoning accuracy. The involvement of grid cells (Schuette et al., 2020), increasingly implicated in abstracting and reasoning two-dimensional information, hints at their potential role in forming and generalizing the two-dimensional fear system in our experimental tasks. Future research should delve deeper into the specific neural mechanisms and explore the intricate interplay between subjective constructs and physiological responses in fear learning.

5. Conclusion

In conclusion, our study demonstrates functional engagement of large-scale brain networks involved in constructing a unified fear space across two dimensions of uncertainty and intensity, suggesting a neurocognitive model through which functional brain networks work in concert to support the construction of a structured representation of fear experiences from multiple dimensions.

CRediT authorship contribution statement

Jing Lyu: Writing – review & editing, Writing – original draft, Visualization, Validation, Supervision, Methodology, Investigation, Formal analysis. **Jiayue Li:** Project administration, Methodology, Investigation, Formal analysis, Data curation, Conceptualization. **Rui Ding:** Visualization, Writing – original draft, Writing – review & editing. **Hui Zhao:** Supervision, Methodology, Data curation, Conceptualization. **Chao Liu:** Conceptualization, Data curation, Formal analysis, Funding acquisition, Methodology. **Shaozheng Qin:** Supervision, Project administration, Methodology, Investigation, Funding acquisition, Data curation.

Ethical approval

The study was granted approval by the Institutional Review Board (IRB) of the State Key Laboratory of Cognitive Neuroscience and Learning at Beijing Normal University.

Declaration of competing interest

The authors have no relevant financial or non-financial interests to disclose.

Acknowledgements

This study received support from STI 2030—Major Projects (2021ZD0200500), the National Natural Science Foundation of China (Grants 32130045, 32361163611, 82021004, and 62077010), the Open Research Fund of the State Key Laboratory of Cognitive Neuroscience and Learning (Grant CNLZD 1503) granted to Shaozheng Qin.

Appendix ASupplementary data

Supplementary data to this article can be found online at https://doi.org/10.1016/j.ynstr.2024.100677.

Data availability

Data will be made available on request.

References

Alvarez, R.P., Biggs, A., Chen, G., Pine, D.S., Grillon, C., 2008. Contextual fear conditioning in humans: cortical-hippocampal and amygdala contributions. J. Neurosci. 28 (24), 6211–6219. https://doi.org/10.1523/JNEUROSCI.1246-08.2008.

Anagnostaras, S.G., Gale, G.D., Fanselow, M.S., 2001. Hippocampus and contextual fear conditioning: recent controversies and advances. Hippocampus 11 (1), 8–17. https://doi.org/10.1002/1098-1063.

Bălan, O., Moise, G., Moldoveanu, A., Leordeanu, M., Moldoveanu, F., 2019. Fear level classification based on emotional dimensions and machine learning techniques. Sensors 19 (7), 1738. https://doi.org/10.3390/s19071738.

Baldi, E., Bucherelli, C., 2014. Entorhinal cortex contribution to contextual fear conditioning extinction and reconsolidation in rats. Neurobiol. Learn. Mem. 110, 64–71. https://doi.org/10.1016/j.nlm.2014.02.004.

Basu, J., Zaremba, J.D., Cheung, S.K., Hitti, F.L., Zemelman, B.V., Losonczy, A., Siegelbaum, S.A., 2016. Gating of hippocampal activity, plasticity, and memory by entorhinal cortex long-range inhibition. Sci. Adv. 351 (6269), aaa5694. https://doi.org/10.1126/science.aaa5694.

Beckers, T., Hermans, D., Lange, I., Luyten, L., Scheveneels, S., Vervliet, B., 2023. Understanding clinical fear and anxiety through the lens of human fear conditioning. Nature Reviews Psychology 2 (4), 233–245. https://doi.org/10.1038/s44159-023-00156-1.

Berboth, S., Morawetz, C., 2021. Amygdala-prefrontal connectivity during emotion regulation: a meta-analysis of psychophysiological interactions. Neuropsychologia 153, 107767. https://doi.org/10.1016/j.neuropsychologia.2021.107767.

Berg, H., Ma, Y., Rueter, A., Kaczkurkin, A., Burton, P.C., DeYoung, C.G., Lissek, S.M., 2021. Salience and central executive networks track overgeneralization of conditioned-fear in post-traumatic stress disorder. Psychol. Med. 51 (15), 2610–2619. https://doi.org/10.1017/S0033291720001166.

Bilodeau-Houle, A., Morand-Beaulieu, S., Bouchard, V., Marin, M.-F., 2023. Parent–child physiological concordance predicts stronger observational fear learning in children with a less secure relationship with their parent. J. Exp. Child Psychol. 226, 105553. https://doi.org/10.1016/j.jecp.2022.105553.

Bishop, S., Duncan, J., Brett, M., Lawrence, A.D., 2004. Prefrontal cortical function and anxiety: controlling attention to threat-related stimuli. Nat. Neurosci. 7 (2), 184–188. https://doi.org/10.1038/nn1173.

Bissière, S., Plachta, N., Hoyer, D., McAllister, K.H., Olpe, H.-R., Grace, A.A., Cryan, J.F., 2008. The rostral anterior cingulate cortex modulates the efficiency of amygdala-dependent fear learning. Biol. Psychiatr. 63 (9), 821–831. https://doi.org/10.1016/j.biopsych.2007.10.022.

Bloom, S.L., 2004. Neither liberty nor safety: the impact of fear on individuals, institutions, and societies, Part I. Psychother. Politics Int. 2 (2), 78–98. https://doi.org/10.1002/ppi.75.

Boddez, Y., Moors, A., Mertens, G., De Houwer, J., 2020. Tackling fear: beyond associative memory activation as the only determinant of fear responding. Neurosci. Biobehav. Rev. 112, 410–419. https://doi.org/10.1016/j.neubiorev.2020.02.009.

Brosnan, M.B., Wiegand, I., 2017. The dorsolateral prefrontal cortex, a dynamic cortical area to enhance top-down attentional control. J. Neurosci. 37 (13), 3445–3446. https://doi.org/10.1523/JNEUROSCI.0136-17.2017.

Chaaya, N., Battle, A.R., Johnson, L.R., 2018. An update on contextual fear memory mechanisms: transition between Amygdala and Hippocampus. Neurosci. Biobehav. Rev. 92, 43–54. https://doi.org/10.1016/j.neubiorev.2018.05.013.

Coutureau, E., Di Scala, G., 2009. Entorhinal cortex and cognition. Prog. Neuro Psychopharmacol. Biol. Psychiatr. 33 (5), 753–761. https://doi.org/10.1016/j.pnpbp.2009.03.038.

Cunningham, W.A., Brosch, T., 2012. Motivational salience: amygdala tuning from traits, needs, values, and goals. Curr. Dir. Psychol. Sci. 21 (1), 54–59. https://doi.org/10.1177/0963721411430832.

Dacey, M., 2019. Simplicity and the meaning of mental association. Erkenntnis 84 (6), 1207–1228.

Deichmann, R., Gottfried, J.A., Hutton, C., Turner, R., 2003. Optimized EPI for fMRI studies of the orbitofrontal cortex. Neuroimage 19 (2), 430–441. https://doi.org/10.1016/S1053-8119(03)00073-9.

Dolcos, F., Iordan, A.D., Dolcos, S., 2011. Neural correlates of emotion–cognition interactions: a review of evidence from brain imaging investigations. J. Cognit. Psychol. 23 (6), 669–694. https://doi.org/10.1080/20445911.2011.594433.

Domjan, M., 2005. Pavlovian conditioning: a functional perspective. Annu. Rev. Psychol. 56, 179–206. https://doi.org/10.1146/annurev.psych.55.090902.141409.

dos Santos Corrêa, M., Grisanti, G.D.V., Franciscatto, I.A.F., Tarumoto, T.S.A., Tiba, P.A., Ferreira, T.L., Fornari, R.V., 2022. Remote contextual fear retrieval engages activity from salience network regions in rats. Neurobiology of Stress 18, 100459. https://doi.org/10.1016/j.ynstr.2022.100459.

Dou, H., Lei, Y., Pan, Y., Li, H., Astikainen, P., 2023. Impact of observational and direct learning on fear conditioning generalization in humans. Prog. Neuro Psychopharmacol. Biol. Psychiatr. 121, 110650. https://doi.org/10.1016/j.pnpbp.2022.110650.

Dunsmoor, J.E., Paz, R., 2015. Fear generalization and anxiety: behavioral and neural mechanisms. Biol. Psychiatr. 78 (5), 336–343. https://doi.org/10.1016/j.biopsych.2015.04.010.

Dymond, S., Dunsmoor, J.E., Vervliet, B., Roche, B., Hermans, D., 2015. Fear generalization in humans: systematic review and implications for anxiety disorder research. Behav. Ther. 46 (5), 561–582. https://doi.org/10.1016/j.beth.2014.10.001.

Eippert, F., Veit, R., Weiskopf, N., Erb, M., Birbaumer, N., Anders, S., 2007. Regulation of emotional responses elicited by threat-related stimuli. Hum. Brain Mapp. 28 (5), 409–423. https://doi.org/10.1002/hbm.20291.

Esteban, O., Markiewicz, C.J., Blair, R.W., Moodie, C.A., Isik, A.I., Erramuzpe, A., Gorgolewski, K.J., 2019. fMRIPrep: a robust preprocessing pipeline for functional MRI. Nature methods 16 (1), 111–116. https://doi.org/10.1038/s41592-018-0235-4.

Feigenberg, J.M., 2014. Nikolai Bernstein-From Reflex to the Model of the Future: from Reflexes to the Model of the Future, vol. 17. LIT Verlag Münster.

Glenn, C.R., Klein, D.N., Lissek, S., Britton, J.C., Pine, D.S., Hajcak, G., 2012. The development of fear learning and generalization in 8–13 year-olds. Dev. Psychobiol. 54 (7), 675–684. https://doi.org/10.1002/dev.20616.

Haselgrove, M., 2016. Overcoming associative learning. J. Comp. Psychol. 130 (3), 226. https://doi.org/10.1037/a0040180.

Hermans, E.J., Kanen, J.W., Tambini, A., Fernández, G., Davachi, L., Phelps, E.A., 2017. Persistence of amygdala–hippocampal connectivity and multi-voxel correlation structures during awake rest after fear learning predicts long-term expression of fear. Cerebr. Cortex 27 (5), 3028–3041. https://doi.org/10.1093/cercor/bhw145.

Höistad, M., Barbas, H., 2008. Sequence of information processing for emotions through pathways linking temporal and insular cortices with the amygdala. Neuroimage 40 (3), 1016–1033. https://doi.org/10.1016/j.neuroimage.2007.12.043.

Ince, S., Steward, T., Harrison, B.J., Jamieson, A.J., Davey, C.G., Agathos, J.A., Felmingham, K.L., 2023. Subcortical contributions to salience network functioning during negative emotional processing. Neuroimage 270, 119964. https://doi.org/10.1016/j.neuroimage.2023.119964.

Jung, J., Ralph, M.A.L., Jackson, R.L., 2022. Subregions of DLPFC display graded yet distinct structural and functional connectivity. J. Neurosci. 42 (15), 3241–3252. https://doi.org/10.1523/JNEUROSCI.1216-21.2022.

Kim, J.J., Jung, M.W., 2006. Neural circuits and mechanisms involved in Pavlovian fear conditioning: a critical review. Neurosci. Biobehav. Rev. 30 (2), 188–202. https://doi.org/10.1016/j.neubiorev.2005.06.005.

Kluen, L.M., Dandolo, L.C., Jocham, G., Schwabe, L., 2019. Dorsolateral prefrontal cortex enables updating of established memories. Cerebr. Cortex 29 (10), 4154–4168. https://doi.org/10.1093/cercor/bhy298.

Kret, M.E., Stekelenburg, J.J., Roelofs, K., De Gelder, B., 2013. Perception of face and body expressions using electromyography, pupillometry and gaze measures. Front. Psychol. 4, 28. https://doi.org/10.3389/fpsyg.2013.00028.

Kroes, M.C., Dunsmoor, J.E., Hakimi, M., Oosterwaal, S., collaboration, N.P., Meager, M. R., Phelps, E.A., 2019. Patients with dorsolateral prefrontal cortex lesions are capable of discriminatory threat learning but appear impaired in cognitive regulation of subjective fear. Soc. Cognit. Affect Neurosci. 14 (6), 601–612. https://doi.org/10.1093/scan/nsz039.

Krolak-Salmon, P., Hénaff, M.A., Isnard, J., Tallon-Baudry, C., Guénot, M., Vighetto, A., Mauguiere, F., 2003. An attention modulated response to disgust in human ventral anterior insula. Ann. Neurol.: Official Journal of the American Neurological Association the Child Neurology Society 53 (4), 446–453. https://doi.org/10.1002/ana.10502.

LaBar, K.S., Cabeza, R., 2006. Cognitive neuroscience of emotional memory. Nat. Rev. Neurosci. 7 (1), 54–64. https://doi.org/10.1038/nrn1825.

LeDoux, J.E., Pine, D.S., 2016. Using neuroscience to help understand fear and anxiety: a two-system framework. Am. J. Psychiatr. 173 (11), 1083–1093. https://doi.org/10.1176/appi.ajp.2016.16030353.

Lissek, S., Biggs, A.L., Rabin, S.J., Cornwell, B.R., Alvarez, R.P., Pine, D.S., Grillon, C., 2008. Generalization of conditioned fear-potentiated startle in humans: experimental validation and clinical relevance. Behav. Res. Ther. 46 (5), 678–687. https://doi.org/10.1016/j.brat.2008.02.005.

Lissek, S., Bradford, D.E., Alvarez, R.P., Burton, P., Espensen-Sturges, T., Reynolds, R.C., Grillon, C., 2014. Neural substrates of classically conditioned fear-generalization in humans: a parametric fMRI study. Soc. Cognit. Affect Neurosci. 9 (8), 1134–1142. https://doi.org/10.1093/scan/nst096.

Liu, Y., Lin, W., Liu, C., et al., 2016. Memory consolidation reconfigures neural pathways involved in the suppression of emotional memories. Nat. Commun. 7, 13375. https://doi.org/10.1038/ncomms13375.

Luo, Y., Qin, S., Fernandez, G., Zhang, Y., Klumpers, F., Li, H., 2014. Emotion perception and executive control interact in the salience network during emotionally charged working memory processing. Hum. Brain Mapp. 35 (11), 5606–5616. https://doi.org/10.1002/hbm.22573.

Maass, A., Schütze, H., Speck, O., Yonelinas, A., Tempelmann, C., Heinze, H.-J., Enno Stephan, K., 2014. Laminar activity in the hippocampus and entorhinal cortex related to novelty and episodic encoding. Nat. Commun. 5 (1), 5547. https://doi.org/10.1038/ncomms6547.

McNally, G.P., Westbrook, R.F., 2006. Predicting danger: the nature, consequences, and neural mechanisms of predictive fear learning. Learn. Mem. 13 (3), 245–253. https://doi.org/10.1101/lm.053894.123.

Menon, V., Uddin, L.Q., 2010. Saliency, switching, attention and control: a network model of insula function. Brain Struct. Funct. 214, 655–667. https://doi.org/10.1007/s00429-010-0262-0.

Mitchell, C.J., De Houwer, J., Lovibond, P.F., 2009. The propositional nature of human associative learning. Behav. Brain Sci. 32 (2), 183–198. https://doi.org/10.1017/S0140525X09000855.

Palaniyappan, L., Liddle, P.F., 2012. Does the salience network play a cardinal role in psychosis? An emerging hypothesis of insular dysfunction. J. Psychiatr. Neurosci. 37 (1), 17–27. https://doi.org/10.1503/jpn.100176.

Pattwell, S.S., Duhoux, S., Hartley, C.A., Johnson, D.C., Jing, D., Elliott, M.D., Yang, R.R., 2012. Altered fear learning across development in both mouse and human. Proc. Natl. Acad. Sci. USA 109 (40), 16318–16323. https://doi.org/10.1073/pnas.1206834109.

Pawliczek, C.M., Derntl, B., Kellermann, T., Kohn, N., Gur, R.C., Habel, U., 2013. Inhibitory control and trait aggression: neural and behavioral insights using the emotional stop signal task. Neuroimage 79, 264–274. https://doi.org/10.1016/j.neuroimage.2013.04.104.

Peers, P.V., Simons, J.S., Lawrence, A.D., 2013. Prefrontal control of attention to threat. Front. Hum. Neurosci. 7, 24. https://doi.org/10.3389/fnhum.2013.00024.

Petrescu, L., Petrescu, C., Oprea, A., Mitruț, O., Moise, G., Moldoveanu, A., Moldoveanu, F., 2021. Machine learning methods for fear classification based on physiological features. Sensors 21 (13), 4519. https://doi.org/10.3390/s21134519.

Rau, V., DeCola, J.P., Fanselow, M.S., 2005. Stress-induced enhancement of fear learning: an animal model of posttraumatic stress disorder. Neurosci. Biobehav. Rev. 29 (8), 1207–1223. https://doi.org/10.1016/j.neubiorev.2005.04.010.

Reilly, J.P., 1998. Sensory Responses to Electrical Stimulation. In: Applied Bioelectricity. Springer, New York, NY. https://doi.org/10.1007/978-1-4612-1664-3_7.

Ridderbusch, I.C., Wroblewski, A., Yang, Y., Richter, J., Hollandt, M., Hamm, A.O., Margraf, J., 2021. Neural adaptation of cingulate and insular activity during delayed fear extinction: a replicable pattern across assessment sites and repeated measurements. Neuroimage 237, 118157. https://doi.org/10.1016/j.neuroimage.2021.118157.

Roesler, R., McGaugh, J.L., 2022. The entorhinal cortex as a gateway for amygdala influences on memory consolidation. Neuroscience 497, 86–96. https://doi.org/10.1016/j.neuroscience.2022.01.023.

Rogan, M.T., Stäubli, U.V., LeDoux, J.E., 1997. Fear conditioning induces associative long-term potentiation in the amygdala. Nature 390 (6660), 604–607. https://doi.org/10.1038/37601.

Ruge, H., Schfer, T., Zwosta, K., Mohr, H., Wolfensteller, U., 2019. Neural representation of newly instructed rule identities during early implementation trials. eLife Sciences 8. https://doi.org/10.7554/eLife.48293.

Schimmelpfennig, J., Topczewski, J., Zajkowski, W., Jankowiak-Siuda, K., 2023. The role of the salience network in cognitive and affective deficits. Front. Hum. Neurosci. 17, 1133367. https://doi.org/10.3389/fnhum.2023.1133367.

Seeley, W.W., 2019. The salience network: a neural system for perceiving and responding to homeostatic demands. J. Neurosci. 39 (50), 9878–9882. https://doi.org/10.1523/JNEUROSCI.1138-17.2019.

Šimić, G., Tkalčić, M., Vukić, V., Mulc, D., Španić, E., Šagud, M., Hof, P.R., 2021. Understanding emotions: origins and roles of the amygdala. Biomolecules 11 (6), 823. https://doi.org/10.3390/biom11060823.

Takehara-Nishiuchi, K., 2014. Entorhinal cortex and consolidated memory. Neurosci. Res. 84, 27–33. https://doi.org/10.1016/j.neures.2014.02.012.

Veit, R., Singh, V., Sitaram, R., Caria, A., Rauss, K., Birbaumer, N., 2012. Using real-time fMRI to learn voluntary regulation of the anterior insula in the presence of threat-related stimuli. Soc. Cognit. Affect Neurosci. 7 (6), 623–634. https://doi.org/10.1093/scan/nsr061.

Verbruggen, F., De Houwer, J., 2007. Do emotional stimuli interfere with response inhibition? Evidence from the stop signal paradigm. Cognit. Emot. 21 (2), 391–403. https://doi.org/10.1080/02699930600625081.

Vogt, B.A., 2019. Cingulate cortex in the three limbic subsystems. Handb. Clin. Neurol. 166, 39–51. https://doi.org/10.1016/B978-0-444-64196-0.00003-0.

Vuilleumier, P., Armony, J., Dolan, R., 2003. Reciprocal links between emotion and attention. Human brain function 2, 419–444. https://doi.org/10.1016/b978-0-444-64196-0.00003-0.

White, L.K., Makhoul, W., Teferi, M., Sheline, Y.I., Balderston, N.L., 2023. The role of dlPFC laterality in the expression and regulation of anxiety. Neuropharmacology 224, 109355. https://doi.org/10.1016/j.neuropharm.2022.109355.

Yin, S., Liu, Y., Petro, N.M., Keil, A., Ding, M., 2018. Amygdala adaptation and temporal dynamics of the salience network in conditioned fear: a single-trial fMRI study. Eneuro 5 (1). https://doi.org/10.1523/ENEURO.0445-17.2018.

Yosephi, M.H., Ehsani, F., Daghiani, M., Zoghi, M., Jaberzadeh, S., 2019. The effects of trans-cranial direct current stimulation intervention on fear: a systematic review of literature. J. Clin. Neurosci. 62, 7–13. https://doi.org/10.1016/j.jocn.2019.01.011.

Zhao, H., Turel, O., Bechara, A., He, Q., 2023. How distinct functional insular subdivisions mediate interacting neurocognitive systems. Cerebr. Cortex 33 (5), 1739–1751. https://doi.org/10.1093/cercor/bhac169.

Zhuang, L., Wang, J., Xiong, B., et al., 2022. Rapid neural reorganization during retrieval practice predicts subsequent long-term retention and false memory. Nat. Hum. Behav. 6, 134–145. https://doi.org/10.1038/s41562-021-01188-4.

Zoladz, P.R., Cordes, C.N., Weiser, J.N., Reneau, K.E., Boaz, K.M., Helwig, S.J., Getnet, B. A., 2023. Pre-learning stress that is temporally removed from acquisition impairs fear learning. Biology 12 (6), 775. https://doi.org/10.3390/biology12060775.